Proceedings of the 27th International Conference *"Mixed Design of Integrated Circuits and Systems"*
June 25-27, 2020, Łódź, Poland

Subband Structure and Ballistic Conductance of a Molybdenum Disulfide Nanoribbon in Topological 1T' Phase: A k·p Study

Viktor Sverdlov
Christian Doppler Laboratory
for Nonvolatile Magnetoresistive Memory and Logic
at the Insitute for Microelectronics
Technische Universität Wien
Vienna, Austria
sverdlov@iue.tuwien.ac.at

Al-Moatasem Bellah El-Sayed, Siegfried Selberherr
Institute for Microelectronics
Technische Universität Wien
Vienna, Austria
el-sayed@iue.tuwien.ac.at, Selberherr@TUWien.ac.at

***Abstract*—We evaluate the subband structure in a narrow nanoribbon of 1T' molybdenum disulfide by employing an effective k·p Hamiltonian. Highly conductive topologically protected edge states whose energies lie within the bulk band gap are investigated. Due to the interaction of the edge modes located at the opposite edges, a small gap in their linear spectrum opens in a narrow nanoribbon. This gap is shown to sharply increase with the perpendicular out-of-plane electric field, in contrast to the behavior in a wide nanoribbon. The gaps between the electron and hole bulk subbands also increase with the electric field. The increase of the gaps between the subbands leads to a rapid decrease of the ballistic nanoribbon conductance and current with the gate voltage, which can be used for designing molybdenum disulfide nanoribbon-based current switches.**

***Keywords*—topological insulators, topologically protected edge states, nanoribbons, subbands, k.p Hamiltonian, ballistic conductance**

I. Introduction

Edge states in two-dimensional (2D) topological insulators (TI) propagate without backscattering, making them attractive for designing highly conductive channels [1]. Recently it was discovered that the 1T' phase of MoS_2, a well-known 2D material with a high promise for future microelectronic devices [2], is a TI [3]. The inverted band structure is well approximated by parabolas, with the conduction and valence bands having masses of $m_{y(x)}^{d(p)}$ [3]. The spin-orbit interaction opens a gap at the intersection of the valence and conduction bands, which appears at a finite value of the momentum k_y along the OY axis. A topologically protected highly conductive edge state with a linear Dirac-like energy dispersion on the momentum k_x parallel to the OX axis must exist within this spin-orbit gap [3].

However, possessing robust conductive channels is only one requirement. To make a good switch it is necessary to suppress the current through the channel as a function of a perpendicular electric field induced by a gate. A standard approach is to close the gap in the bulk host material. In this case scattering between the protected edge and the non-protected electron-hole bulk states results in strong scattering, which effectively reduces the current through the edge states [4].

By applying an electric field E_z along the OZ axis perpendicular to a MoS_2 sheet in the 1T' phase, the bulk spin-orbit gap can be reduced, closed, and opened again as a "negative" gap at large electric fields [3]. The traditional band order is restored from the inverted band structure, the gap becomes a direct gap, and no edge states are allowed in the gap.

This transition between the topological and conventional insulator phases in a wide1T'-MoS_2 controlled by the electric field orthogonal to the sheet eliminates the edge states completely and can be used to further suppress the current [5]. In order to enhance the current through the channel it is beneficiary to have many edges by stacking several narrow nanoribbons. Here, we evaluate the subband structure in a narrow nanoribbon of 1T'-MoS_2 by using an effective k·p Hamiltonian [3]. In contrast to a wide channel, we find that a small gap in the spectrum of edge states in a nanoribbon [6] increases with the electric field. It results in a rapid decrease in the nanoribbon conductance with the field, which is potentially suitable for switching.

II. Method and Results

In order to investigate transport through a nanoribbon, the subband structure and the wave functions must be evaluated first. We parametrize the energy in units of the band inversion gap 2δ at k_y=0, while $k_{y(x)}$ in units of $k_0 = \left(\frac{4\delta}{\hbar^2}\frac{m_y^d m_y^p}{m_y^d+m_y^p}\right)^{1/2}$. By applying a unitary transformation [7] , the 4×4 Hamiltonian [3] is cast in a block-diagonal form similar to the one in [6].

$$\begin{pmatrix} H(\mathbf{k}) & 0 \\ 0 & H^*(-\mathbf{k}) \end{pmatrix} \quad (1)$$

The 2×2 Hamiltonian $H(\mathbf{k})$,$\mathbf{k}$=(k_x, k_y) in dimensionless units has the form

$$H(\mathbf{k}) = \begin{pmatrix} \frac{1}{2} - k_y^2\frac{m}{m_y^p} - k_x^2\frac{m}{m_x^p} & v_2 k_y - \alpha E_z + i\, v_1 k_x \\ v_2 k_y - \alpha E_z - i\, v_1 k_x & -\frac{1}{2} + k_y^2\frac{m}{m_y^d} + k_x^2\frac{m}{m_x^d} \end{pmatrix}, \quad (2)$$

where $m = \frac{m_y^d m_y^p}{m_y^d+m_y^p}$ and $v_{1(2)}$ are the dimensionless velocities. The parameters used in (2) are from [3] and listed in Table I.

The bulk energy dispersion obtained with the Hamiltonian (2) with an offset of $\Delta E = \frac{1}{2}\frac{m_y^d - m_y^p}{m_y^d+m_y^p}$ is shown in Fig. 1 for several k_x and E_z=0. The spin-orbit gap opened at $k_y = \pm k_0$ is increasing with k_x. Indeed, the gap is determined by the off-diagonal terms in (2). Since the off-diagonal terms in (2) can be written as $\sigma_y v_1 k_x$ and $\sigma_x v_2 k_y$, where $\sigma_{x(y)}$ are the Pauli matrices, the gap Δ is defined by $\Delta=(v_1^2 {k_x}^2 + v_2^2 {k_y}^2)^{1/2}$.

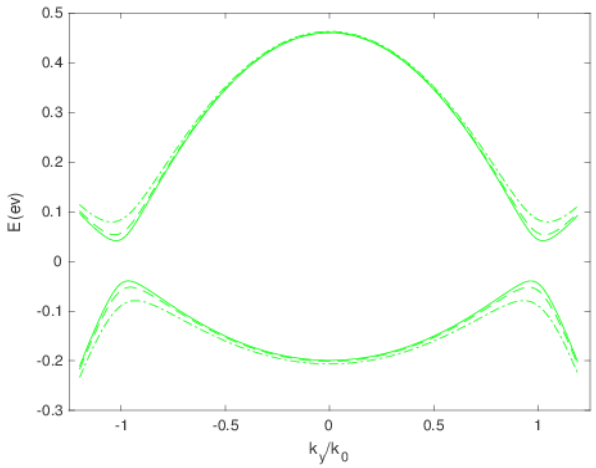

Fig. 1. Bulk energy dispersion in 1T'-MoS_2 two-dimensional material, E_z=0, for k_x=0 (solid line), k_x=0.1 k_0 (dashed line), and k_x=0.2 k_0 (dot-dashed line).

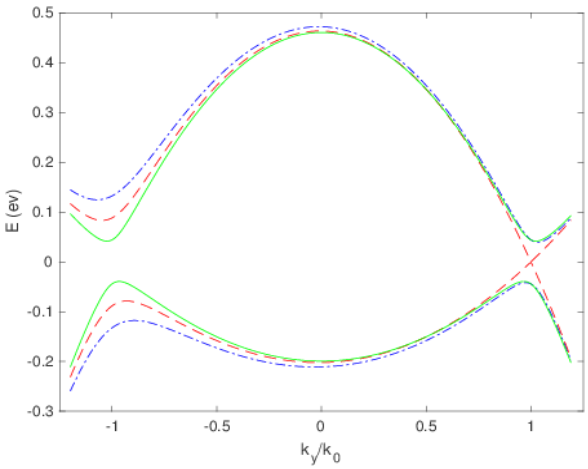

Fig. 2. Bulk energy dispersion in 1T'-MoS_2 two-dimensional material, k_x=0, for E_z=0 (solid line), αE_z=v_2 (dashed line) and αE_z=2v_2 (dot-dashed line).

By applying an electric field E_z along the OZ axis the gap at one of the minima (Fig.2, solid line) can be reduced, completely closed (Fig.2, dashed line), or even be opened again (Fig.1, dot-dashed line) at large electric fields. The gap at large electric fields becomes direct.

Let us consider a nanoribbon with a width in the OY direction of d=40/k_0. Only quantized values of the momentum k_y along the quantization axis OY are allowed. In addition, it is expected that at E_z =0 two topologically protected highly conductive edge states localized at opposite interfaces of a nanoribbon exist at any particular energy E within the gap opened by the spin-orbit interaction at k_y =± k_0.

A general form of the subband wave function $\psi_{k_x}(y)$ in the quantization OY direction is written as

$$\psi_{k_x}(y) = \sum_{j=1}^{4} A_j \begin{pmatrix} 1 \\ a(k_j, E) \end{pmatrix} \exp(ik_j y), \qquad (3)$$

where k_j, j=1,…,4 are the roots of $E(k_x, k_j)$= E, A_j are constants, and

$$a(k_j, E) = \frac{-\frac{1}{2} + k_j^2 \frac{m}{m_y^p} + k_x^2 \frac{m}{m_x^p} + E}{v_2 k_j - \alpha E_z + i\, v_1 k_x}. \qquad (4)$$

The subband energies are obtained by setting the wave function to zero at both edges. The characteristic equation

$$\det(\mathbf{M}) = 0, \qquad (5)$$

where the matrix $\mathbf{M} = (M_1 \quad M_2 \quad M_3 \quad M_4)$ is composed of the columns M_j, j=1,..,4.

$$M_j = \begin{pmatrix} 1 \\ a(k_j, E) \\ \exp(ik_j d) \\ a(k_j, E)\exp(ik_j d) \end{pmatrix}, \qquad (6)$$

is solved numerically, in complete analogy to the problem of finding the eigenenergies and eigenfunctions of a 2-band **k·p** Hamiltonian in silicon films [8]. Fig.3 displays the behaviour of the real part (the imaginary part is zero for E_z=0) of the determinant as a function of energy, for k_x=0. We are interested

TABLE I.
PARAMETERS [3,5] USED IN THE MODEL. m_e IS THE ELECTRON MASS, e IS THE ELECTRON CHARGE, AND d IS THE WIDTH IN OY DIRECTION.

Variable	Value
2δ	0.66 eV
v_1	3.87 10^5 m/s
v_2	0.46 10^5 m/s
m_x^p	0.5 m_e
m_y^p	0.16 m_e
m_x^d	2.48 m_e
m_y^d	0.37 m_e
α	0.03 e nm
k_0	1.485 nm^{-1}
d	$40k_0^{-1}$ = 26.94 nm

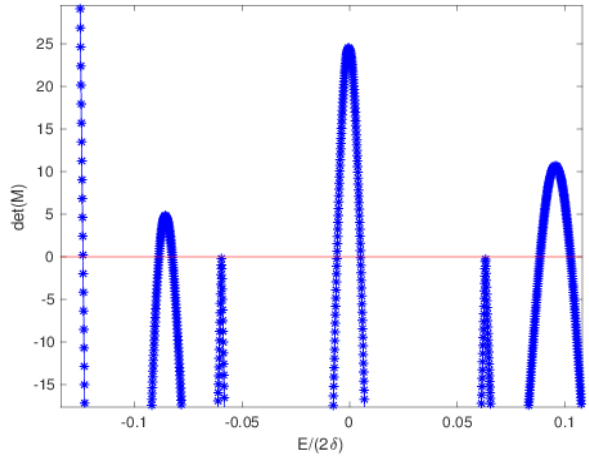

Fig. 3. Real (stars) and imaginary (line) parts of det(**M**) computed at k_x =0, E_z = 0, d=40k_0^{-1}. The bulk gap is seen at at E ≈ ±0.065, where the real part touches the OX axis from below. The subband energies are obtained from det(**M**)=0. Topological edge states are seen in the bulk gap (E ≈ ±0.005).

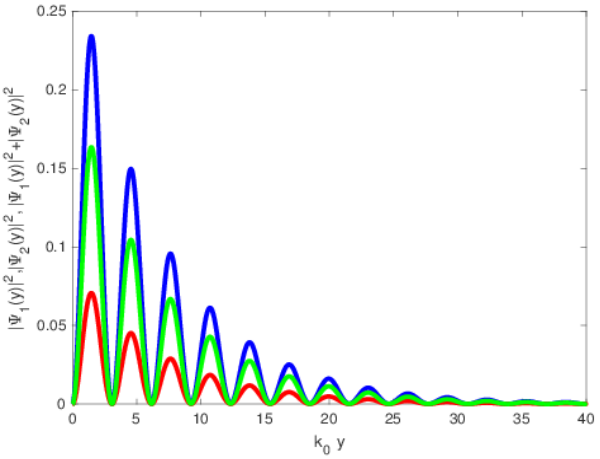

Fig. 4. The wave function square (blue) and its two spinor components (green and red) of the topological edge state evaluated at $\alpha E_z = 0.1v_2$, $k_x = 0.1k_0$, and $E \approx 0.005$. The subband wave function shows both oscillation and an exponential decay.

in the crossings of the curve with the axis OX. The bulk gap due to the spin-orbit interaction occurs at $E \approx \pm 0.065$. The value of the determinant approaches zero from negative values and touches it at a single point, when the energy E touches the minimum (maximum) of the dispersion curve. Therefore, $k_1 = k_2$ and $k_3 = k_4$ and the determinant (5) is zero.

All other intersections with the OX axis correspond to subband energies. We clearly observe two roots in the gap at $E \approx \pm 0.005$ A close inspection shows that the wave vectors k_j corresponding to these solutions are complex numbers. The wave functions corresponding to these solutions in the gap are located at an edge of the nanoribbon as shown in Fig.4 and Fig.5 for $k_x = 0.1k_0$ and $E \approx \pm 0.005$, respectively. In contrast to [6], where only an exponential decay was predicted, the wave functions display both oscillations and decay. Although the structure of the Hamiltonians considered here and in [6] are similar, the actual parameters differ. In particular, here the spin-orbit gaps are open at the finite values of $k_y = \pm k_0$. This displacement of the bulk band's minima from the Gamma-point at $k_y = 0$ is reflected in the oscillations of subband wave functions superimposed on the exponential decay.

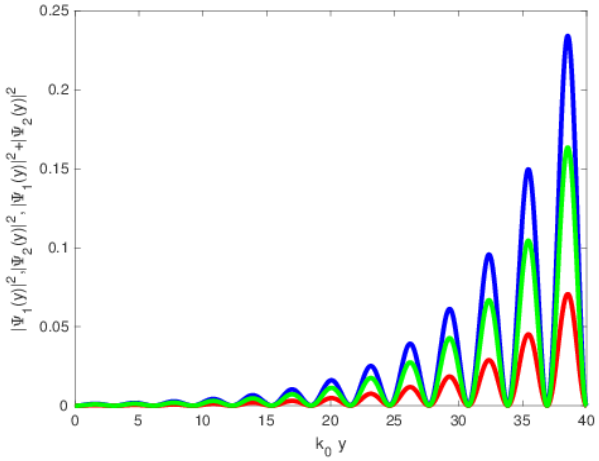

Fig. 5. The wave function square (blue) and its two spinor components (green and red) of the topological edge state evaluated at $\alpha E_z = 0.1v_2$, $k_x = 0.1k_0$, but $E \approx -0.005$. The wave function is localized at the oppoite edge.

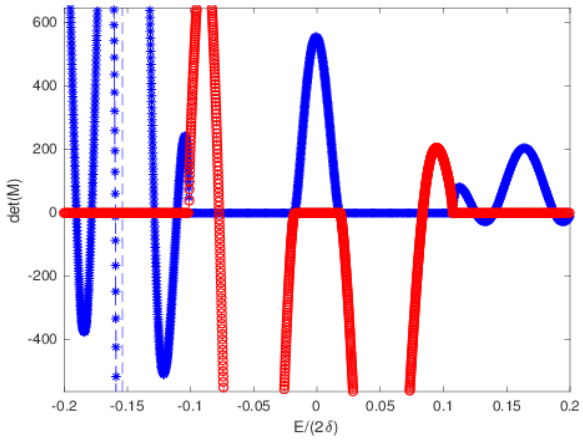

Fig.6 Real (blue stars) and imaginary (red circles) parts of det(**M**) computed at $k_x = 0$, $\alpha E_z = 0.7\, v_2$, $d = 40k_0^{-1}$. At $E \approx \pm 0.02$ the imaginary part of the two k_j ensuring the localization at the edges is approaching zero. New type of roots with imaginary part equals to zero at $E \approx \pm 0.075$ appear.

The roots of the determinant for $|E| > 0.065$ correspond to the subbands with all k_j real. The wave functions are delocalised through the width of the nanoribbon. Due to the strong non-parabolicity of the bulk dispersion, the positions of the subband minima and the subband dispersions can only be found by solving (5) numerically.

Fig. 6 shows the behavior of the determinant at $\alpha E_z = 0.7 v_2 \hbar k_0$. In this case the gap at $k = k_0$ is reduced but not completely closed. However, due to the finite width of the nanoribbon, the edge modes seen at $E \approx \pm 0.02$ are already delocalized as the imaginary parts of two k_j responsible for the localization at the edges are becoming zero. At the same time, the two solutions at $E \approx \pm 0.075$ split off from the traditional subbands set as two of their k_j acquire an imaginary part. This happens due to the fact that, while the gap at $k_y = k_0$ shrinks with increasing E_z, the gap at $k_y = -k_0$ displays an opposite trend and becomes wider. Therefore, the lowest traditional subband initially outside of the gap enters the gap at $k_y = -k_0$ thus forcing the two roots to become complex.

The behaviour of the determinant at even higher electric field $\alpha E_z = 1.4 v_2 \hbar k_0$ is shown in Fig.7. As the field is larger than the

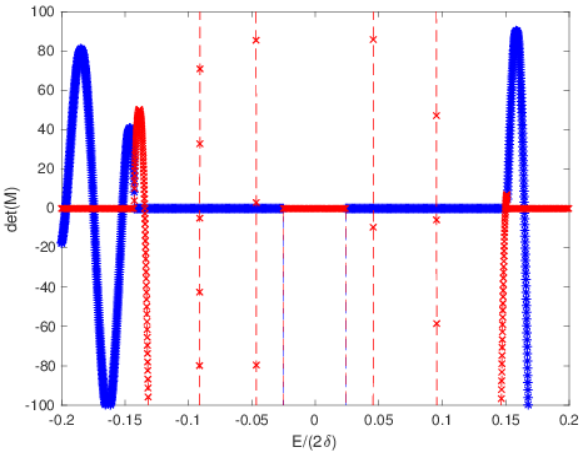

Fig.7. Real (blue stars) and imaginary (red crosses) parts of det(**M**) computed at $k_x = 0$, $\alpha E_z = 1.7 v_2$, $d = 40k_0^{-1}$. No solution within the direct gap at $|E| < 0.03$ is allowed. Two solutions of with imaginary part equal to zero at $E \approx \pm 0.05$ and $E \approx \pm 0.08$ are now observed.

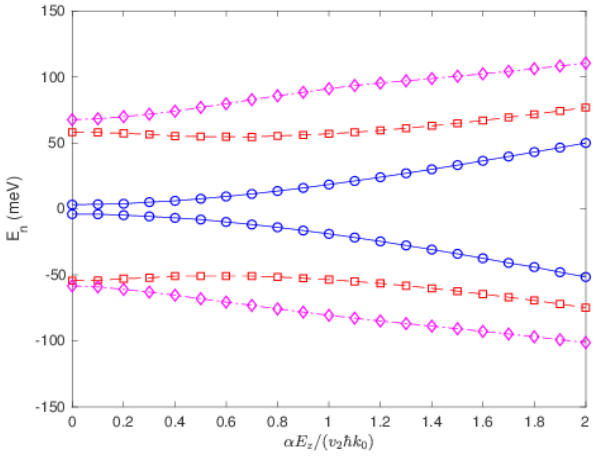

Fig. 8. Dependence of electron (hole) subband minima (maxima) on the electric field E_z for the first three subbands. In contrast to the bulk case, the gap never closes and keeps increasing with E_z

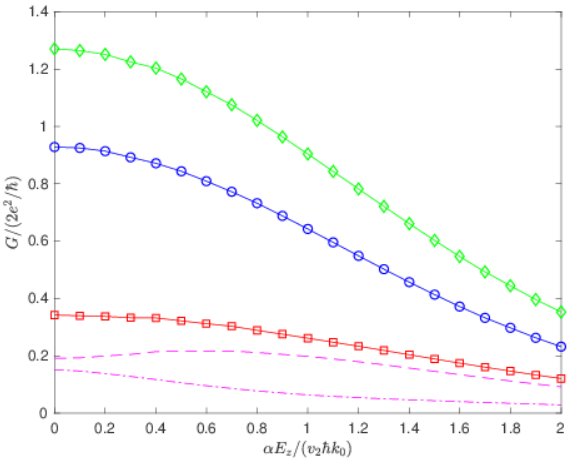

Fig. 9. Ballistic conductance (diamonds) of a 1T'-MoS_2 nanoribbon, with the contributions from the edge-like states (circles), and the remaining bulk-like subbands (squares). Dashed line from subbands shown in Fig.8 by squares; dot-dashed line from Fig.8, diamonds. Temperature T=300K, E_F=0

critical value field $\alpha E_z = v_2\hbar k_0$ at which there is no gap at $k_y = k_0$, the gap seen att $|E|<0.03$ is a direct gap. Therefore, as confirmed by the absence of zeroes of the determinant, no edge states are allowed in the gap. At the same time, there are already four subbands lying outside the direct gap at $k_y = k_0$ but still within the gap at $k_y = -k_0$. While the solutions at $E \approx \pm 0.09$ split off from the traditional subbands set in complete analogy to the situation in Fig. 6, the subbands at $E \approx \pm 0.05$ originate in the edge states, which were continuously pushed outside of the gap at $k_y = -k_0$.

Fig.8 shows the dependence of the electron (hole) subband minima (maxima) $E_n^{e(h)}$ on the electric field E_z. First, we note that the "bulk" gap in the nanoribbon defined as the difference between the extrema of the first traditional subbands (Fig.8, squares) shows signs of reduction, when the field is increased till $E_z \approx 0.7 v_2\hbar k_0/\alpha$, after which the trend is inverted. This behavior is in sharp contrast to that in wide ribbons in which the bulk gap closes at $E_z = v_2\hbar k_0/\alpha$ (Fig.1, dashed line).

Second, with increasing E_z the gap between the lowest electron and the highest edge-like subbands grows (Fig. 8, circles). As indicated in Fig.5 and Fig.6, all four k_j contain an imaginary part for $E_z < 0.7 v_2\hbar k_0/\alpha$. This value is lower than the value $E_z < v_2\hbar k_0/\alpha$ corresponding to the bands' inversion in the bulk. The increasing gap between the edge-like subbands is reflected in the decrease of the corresponding nanoribbon ballistic conductance shown in Fig.9 (circles). Although the edge-like subbands give the leading contribution in the conductance G (Fig.9, diamonds) computed as

$$G = \frac{2e^2}{h}\sum_j \left[\frac{1}{\exp\left\{\frac{E_i^e - E_F}{k_B T}\right\}+1} - \frac{1}{\exp\left\{\frac{E_i^h - E_F}{k_B T}\right\}+1} + 1\right], \qquad (7)$$

where T is the temperature and E_F is the Fermi energy, the role of the other subbands shown in Fig.9 by squares is non-negligible. The first two electron (hole) bulk-like subbands give similar contributions to the ballistic conductance totaling to 30%. However, all contributions to the total conductance G rapidly decrease as a function of E_z (Fig.9). This makes 1T'-MoS_2 potentially suitable for switching applications.

Acknowledgment

Financial support by the Austrian Federal Ministry for Digital and Economic Affairs and the National Foundation for Research, Technology and Development is gratefully acknowledged. A.-M.B.E.-S. was supported in part by project No. IN 23/2018 'Atom-to-Circuit modeling technique for exploration of Topological Insulator based ultra-low power electronics' by the Centre for International Cooperation & Mobility (ICM) of the Austrian Agency for International Cooperation in Education and Research (OeAD).

References

[1] L. Kou, Y. Ma, Z. Sun, T. Heine, and C. Chen,"Two-dimensional topological insulators: Progress and prospects", J.Phys.Chem.Lett. vol.8, pp.1905-1919, 2017.

[2] Yu.Yu. Illarionov, A.G. Banshchikov, D.K. Polyushkin, S. Wachter, T. Knobloch, M. Thesberg, L. Mennel, M. Paur, M. Stöger-Pollach, A. Steiger-Thirsfeld, M.I. Vexler, M. Waltl, N.S. Sokolov, T. Mueller, and T. Grasser, "Ultrathin calcium fluoride insulators for two-dimensional field-effect transistors", Nature Electronics, vol.2, pp.230-235, 2019.

[3] X. Qian, J. Liu, L. Fu, and Ju Li., "Quantum spin Hall effect in two-dimensional transition metal dichalcogenides", Science, vol. 346, issue 6215, pp.1344-1347, 2014.

[4] W.G.Vandenberghe and M. V. Fischetti, "Imperfect two-dimensional topological insulator field-effect transistors", Nature Communications. Vol.8, art.14184 (pp. 1-8), 2017.

[5] L. Liu and J. Guo, "Assessment of performance potential of MoS_2-based topological insulator field-effect transistors", J.Appl.Phys., vol.118, art.124502 (pp.1-5), 2015.

[6] B. Zhou, H.-Z. Lu, R.-L. Chu, S.-Q. Shen, and Q. Niu, "Finite size effects on helical edge states in a quantum spin-Hall system" Phys.Rev.Lett., vol.101, art.246807 (pp.1-4), 2008.

[7] V. Sverdlov, A.-M.B. El-Sayed, H. Kosina, and S. Selberherr, "Topologically protected and conventional subbands in a 1T'-MoS_2 nanoribbon channel", EUROSOI-ULIS 2020, accepted.

[8] V. Sverdlov and S. Selberherr, "Silicon spintronics: Progress and challenges", Phys.Rep., vol.585, pp.1-40, 2015.